3-1-2021

Nighttime Magnetic Perturbation Events Observed in Arctic Canada: 3. Occurrence and Amplitude as Functions of Magnetic Latitude, Local Time, and Magnetic Disturbance Indices

Mark J. Engebretson
Augsburg University, engebret@augsburg.edu

Viacheslav A. Pilipenko
Augsburg University, pilipenk@augsburg.edu

Erik S. Steinmetz
Augsburg University, steinmee@augsburg.edu

Mark B. Moldwin
University of Michigan, Ann Arbor

Martin G. Connors
Athabasca University

Follow this and additional works at: https://idun.augsburg.edu/faculty_scholarship
See next page for additional authors
Part of the Physics Commons

Recommended Citation

Authors

Mark J. Engebretson, Viacheslav A. Pilipenko, Erik S. Steinmetz, Mark B. Moldwin, Martin G. Connors, David H. Boteler, Howard J. Singer, Hermann Opgenoorth, Audrey Schillings, Shin Ohtani, Jesper Gjerloev, and Christopher T. Russell

Key Points:
- We present 2 years of observations of ≥6 nT/s magnetic perturbation events (MPEs) from five high-latitude Arctic stations
- Most MPEs occurred within 30 min of a substorm onset, but substorms were neither necessary nor sufficient to cause MPEs
- Pre- and postmidnight MPEs had different temporal relations to substorms and occurred at slightly different latitudes

Nighttime Magnetic Perturbation Events Observed in Arctic Canada: 3. Occurrence and Amplitude as Functions of Magnetic Latitude, Local Time, and Magnetic Disturbance Indices

Mark J. Engebretson[1] , Viacheslav A. Pilipenko[1,2] , Erik S. Steinmetz[1] , Mark B. Moldwin[3] , Martin G. Connors[4] , David H. Boteler[5] , Howard J. Singer[6] , Hermann Opgenoorth[7] , Audrey Schillings[7] , Shin Ohtani[8] , Jesper Gjerloev[8] , and Christopher T. Russell[9]

[1]Augsburg University, Minneapolis, MN, USA, [2]Institute of Physics of the Earth, Moscow, Russia, [3]University of Michigan, Ann Arbor, MI, USA, [4]Athabasca University, Athabasca, AB, Canada, [5]Natural Resources Canada, Ottawa, ON, Canada, [6]NOAA Space Weather Prediction Center, Boulder, CO, USA, [7]Umeå University, Umeå, Sweden, [8]JHU/APL, Laurel, MD, USA, [9]UCLA Department of Earth Planetary and Space Sciences, Los Angeles, CA, USA

Abstract Rapid changes of magnetic fields associated with nighttime magnetic perturbation events (MPEs) with amplitudes $|\Delta B|$ of hundreds of nT and 5–10 min duration can induce geomagnetically induced currents (GICs) that can harm technological systems. This study compares the occurrence and amplitude of nighttime MPEs with $|dB/dt| \geq 6$ nT/s observed during 2015 and 2017 at five stations in Arctic Canada ranging from 64.7° to 75.2° in corrected geomagnetic latitude (MLAT) as functions of magnetic local time (MLT), the SME (SuperMAG version of AE) and SYM/H magnetic indices, and time delay after substorm onsets. Although most MPEs occurred within 30 min after a substorm onset, ∼10% of those observed at the four lower latitude stations occurred over two hours after the most recent onset. A broad distribution in local time appeared at all five stations between 1700 and 0100 MLT, and a narrower distribution appeared at the lower latitude stations between 0200 and 0700 MLT. There was little or no correlation between MPE amplitude and the SYM/H index; most MPEs at all stations occurred for SYM/H values between −40 and 0 nT. SME index values for MPEs observed >1 h after the most recent substorm onset fell in the lower half of the range of SME values for events during substorms, and dipolarizations in synchronous orbit at GOES 13 during these events were weaker or more often nonexistent. These observations suggest that substorms are neither necessary nor sufficient to cause MPEs, and hence predictions of GICs cannot focus solely on substorms.

1. Introduction

Although evidence of the impact of solar disturbances on technological systems on Earth arguably goes back to the Carrington event of 1859 (Carrington, 1860), in which a large and complex set of solar flares caused disturbances in telegraph systems over a large portion of the Earth, the developing scientific understanding of the connection between "space weather" and its impacts on human technological systems is still incomplete. It is now understood that the interaction of solar wind plasmas with the near-Earth space environment drives geomagnetic storms, substorms, and large-scale current systems in the magnetosphere and ionosphere, and that transient currents in the ionosphere can drive large and damaging geomagnetically induced currents (GICs) in long-distance electrical power lines and pipelines (Boteler et al., 1998; Kappenman, 2005; Knipp, 2015).

Early studies of the magnetic perturbations that are signatures of these transient ionospheric currents noted the small-scale character of these events (e.g., Viljanen, 1997), but many efforts to predict GICs have continued to focus on global processes (geomagnetic storms and substorms). Recent observational studies by Ngwira et al. (2015, 2018), Belakhovsky et al. (2019), Dimmock et al. (2019, 2020), and Apatenkov et al. (2020) have provided new evidence of the localized nature of the magnetospheric and/or ionospheric processes associated with these impulsive magnetic perturbations. This includes evidence of ionospheric

current vortices, their close association with transient overhead north-south oriented auroral structures and poleward boundary intensifications, and information on the spatial scale size of individual events.

This paper is the third in a series of observational studies of large, impulsive nighttime magnetic perturbations, unipolar or bipolar pulses of hundreds of nT and ~5–10 min duration that we have designated as MPEs, observed in data from a large two-dimensional array of ground-based magnetometers centered in eastern Arctic Canada. The first paper in this series, Engebretson, Pilipenko, et al. (2019), henceforth designated as paper 1, presented statistical results from eight stations covering a range of magnetic latitudes from 68° to 78°. Paper 1 reported, among other results, that most but not all MPEs in this data set were temporally associated with substorms, that their association with magnetic storms was much lower above 73° magnetic latitude, and that MPEs had a half-amplitude horizontal radius of ~275 km. The second paper (Engebretson, Steinmetz, et al., 2019), henceforth designated as paper 2, presented case studies of three intervals containing MPEs using data from a larger set of magnetometers, augmented by observations from auroral imagers and high-altitude spacecraft in the nightside magnetosphere. MPEs were found to be closely associated with transient overhead north-south oriented auroral structures and less closely associated with substorm onsets.

A more recent paper (Engebretson et al., 2020) reported case studies of four intervals containing MPEs using data from magnetometers in Western Greenland and eastern Arctic Canada as well as magnetically conjugate sites in Antarctica. This paper found that conjugate premidnight MPEs were often but not always simultaneous to within 3 min over ~100–700 km in latitude, while postmidnight MPEs associated with an omega band were very localized and independent in time. Analysis of these events also showed that both perturbation amplitudes and maximum derivatives favored a current generator model over a voltage generator model for near-solstice events.

In this study, we present additional analyses of a large number of nighttime MPEs at five of the stations in Arctic Canada used in papers 1 and 2. In addition to comparisons with the SYM/H index (a 1-min cadence proxy for geomagnetic storm intensity) and near-tail dipolarizations (rapid northward turnings of the magnetic field that are a signature of reconnection in the magnetotail), we use two data products developed by the SuperMAG project at the Johns Hopkins University Applied Physics Laboratory (http://supermag.jhuapl.edu): the 1-min cadence SME index (the SuperMAG version of the Auroral Electrojet [AE] index, described in Newell & Gjerloev, 2011a), and the SuperMAG list of substorms. This paper documents the lack of any close correlation between MPE occurrence and levels of the SME index, the SYM/H index, or near-tail dipolarizations, and shows in more detail that a substantial fraction of these events are not temporally associated with substorms. In addition, we show that MPEs occurring in the postmidnight sector had a different dependence on both latitude and prior substorm activity than did the more numerous premidnight MPEs.

Section 2 describes the data used in this study and the procedure used to identify and quantify MPEs. Section 3 presents the occurrence and amplitude distributions of MPEs at each station as a function of time delay after substorm onset, and Section 4 presents the distribution of MPE occurrences as a function of their amplitude in three categories of time delay after substorm onset. Section 5 presents distributions of MPE occurrences and amplitudes as a function of MLT and the SYM/H and SME indices. Section 6 provides more details of the occurrences of MPEs in relation to substorms and magnetotail dipolarizations. Section 7 summarizes the above observations, and Section 8 places these observations in the context of other recent studies and open questions and presents our conclusions.

2. Data Set and Event Identification Technique

Vector magnetometer data used in this study were recorded during 2015 and 2017 by stations in the MACCS (Engebretson et al., 1995), CANMOS (Nikitina et al., 2016), and AUTUMNX (Connors et al., 2016) arrays in Arctic Canada, as detailed in Table 1 and Figure 1 (red circles). MACCS station CDR and the highest and lowest latitude stations in the AUTUMNX array, SALU and KJPK, form a latitudinal chain. MACCS station RBY extends this chain to the north and west, and CANMOS station IQA extends it to the east. Data from 2016 were not included because of significant station down time at RBY and CDR during that year. Also shown in Figure 1 (yellow circle) is the approximate northern magnetic footpoint of the geosynchronous

Table 1
Locations of the Magnetometer Stations Used in This Study

Array	Station	Code	Geog Lat	Geog Lon	CGM Lat	CGM Lon	UT of Mag Noon	Cadence, s
MACCS	Repulse Bay	RBY	66.5°	273.8°	75.2°	−12.8°	17:47	0.5
	Cape Dorset	CDR	64.2°	283.4°	72.7°	3.0°	16:58	0.5
CANMOS	Iqaluit	IQA	63.8°	291.5°	71.4°	15.1°	16:19	1.0
AUTUMNX	Salluit	SALU	62.2°	284.3°	70.7°	4.1°	16:54	0.5
	Kuujuarapik	KJPK	55.3°	282.2°	64.7°	0.2°	17.06	0.5

Notes. Geographic and corrected geomagnetic (CGM) latitude and longitude are shown, as well as the universal time (UT) of local magnetic noon. CGM coordinates were calculated for epoch 2015, using http://sdnet.thayer.dartmouth.edu/aacgm/aacgm_calc.php%23AACGM.

GOES 13 spacecraft (Singer et al., 1996), which provides magnetospheric context for the ground observations. This footpoint, determined via SSCWEB for year 2015 (https://sscweb.gsfc.nasa.gov/), varies daily and seasonally from ~2° geographic north of the Belcher Islands (as shown) to ~1° south, and ~1° east to ~2° west of these islands.

The semi-automated procedure used to identify and quantify MPEs in these data sets is detailed in paper 1, and is summarized here. Routinely produced daily magnetograms (24-h plots of magnetic fields in local geomagnetic coordinates (B_x northward, B_y eastward, and B_z vertically downward) were displayed on a computer screen. Once a < 10 min duration magnetic perturbation with amplitude ≥ 200 nT in any component
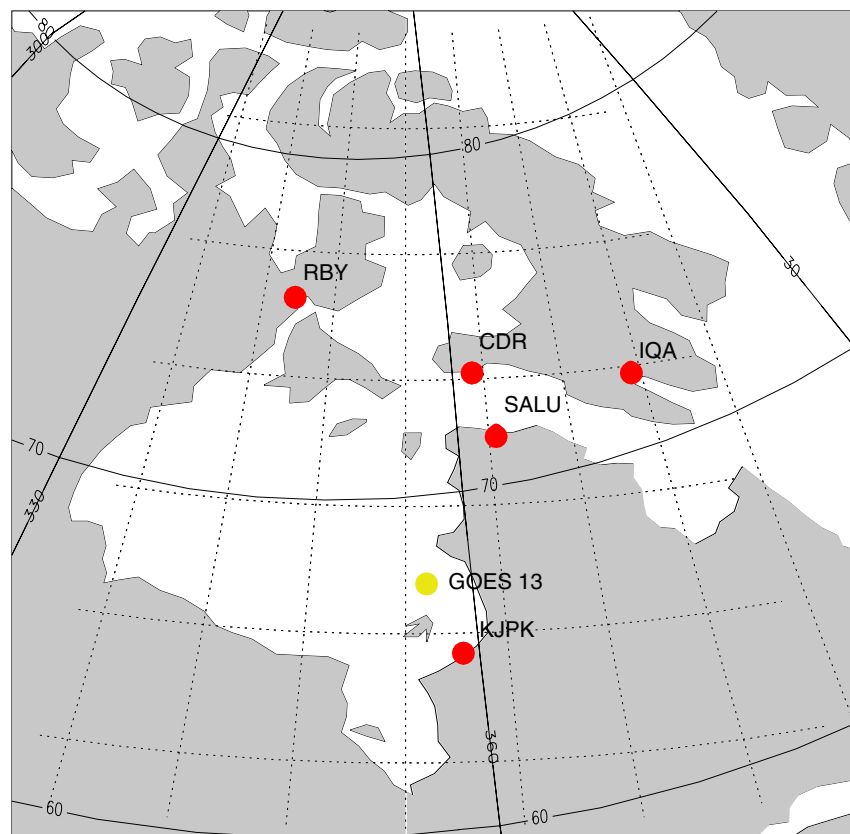

Figure 1. Map of Eastern Arctic Canada showing the location of the five ground magnetometers that provided data for this study. Also shown by the yellow circle is the approximate northern magnetic footpoint of the geosynchronous GOES-13 spacecraft. Solid lines show corrected geomagnetic coordinates.

was identified a cursor pick function was used to visually select times before and after a region of interest containing the MPE (typically with 1–2 h duration). The times and values of extrema in this interval were recorded for each component, and after application of a 10-point smoothing to reduce noise and eliminate isolated bad data points, the data were numerically differentiated. Plots of the time series of data and derivatives were produced and saved, and the maximum and minimum derivative values were automatically determined and recorded. Figure 3 of paper 1 shows the amplitude versus MLT distributions of MPEs at SALU during 2015 for both the perturbation amplitude ΔB_x and the maximum of the derivative $|\mathrm{d}B_x/\mathrm{d}t|$ that were identified using this technique. This figure shows that MPEs with ΔB_x amplitude ≥ 200 nT or derivative amplitude ≥ 6 nT/s were almost exclusively confined to nighttime hours.

The MPE occurrences at each station were compared with the list of interplanetary shocks compiled by Oliveira et al. (2018) in order to identify externally triggered events. Only one nighttime MPE event coincided with a shock event within 30 min and was removed from our database.

We then compared the time of each MPE identified during full years 2015 and 2017 at each station to the times of substorm onsets listed in the SuperMAG substorm list for that year. The procedure used to identify substorm onsets included in the SuperMAG substorm lists is described in Newell and Gjerloev (2011a, 2011b): substorm onsets are defined by a drop in SML (the SuperMAG version of the AL index) that was sharp (45 nT in 3 min) and that was sustained (−100 nT average for 25 min starting 5 min after onset). Onsets are relatively easy to identify if preceded by quiet periods, but subsequent onsets (which may be called intensifications) are far more difficult to identify using either ground-based magnetometer data or auroral images. We note also that in contrast to these step function-like criteria for onsets, the large nighttime MPEs that are the focus of this series of papers are unipolar or bipolar and of shorter duration. We identified and recorded the time of all prior substorm onsets within a 2-h window, and if none were found, the time of the closest prior onset, which in some cases was several days prior to the MPE. Table 2 shows the number of nighttime (1700–0700 MLT) MPEs with derivative amplitude ≥ 6 nT/s at each of these stations. Events are grouped into three categories of time delay Δt after the most recent prior substorm onset: $\Delta t \leq 30$ min, $30 < \Delta t < 60$ min, and $\Delta t \geq 60$ min. In this study, we define events with $\Delta t \leq 30$ min as most likely to be associated with substorm processes, while those with $\Delta t \geq 60$ min (and up to several days) are not. The fractions of events that occurred in these three different delay ranges remained roughly constant at all stations. Note, too, that the total number of events (280) peaked at SALU (70.7° MLAT), and was much lower (84 and 122) at the two latitude extremes, RBY (75.2° MLAT) and KJPK (64.7° MLAT), respectively.

3. MPE Amplitudes as a Function of Time Delay After Substorm Onset

Figure 2 shows the amplitude of the maximum $|\mathrm{d}B/\mathrm{d}t|$ value in any nighttime MPE component observed at each station as a function of its delay (between 0 and 120 min) after the most recent substorm onset. The small number of events with the largest $|\mathrm{d}B/\mathrm{d}t|$ values (≥ 20 nT/s) most often appeared after shorter postonset delays. Most events were below 12 nT/s for all delay times. MPEs occurred over a continuum of times from 0 to well beyond the 120 min delay time range shown in this figure. The number and percentage of events occurring with delay times >120 min are indicated in the inset box in each panel. Although most MPEs at each station occurred within 30 min after a substorm onset, from 13% to 20% of the MPEs at each station occurred later than 1 h after the most recent substorm onset, and from 6% to 12% later than 2 h. The number of events >10 nT/s with time delays over two hours was 0 at RBY and CDR, 1 at IQA, 5 at SALU, and 3 at KJPK (not shown).

Figure 2 was prepared without regard to the distance in MLT between a substorm onset and an MPE. Gjerloev et al. (2004), following an earlier study by Kamide and Kokubun (1996), showed the difficulties in accurately determining the location of substorm onsets using only ground-based magnetometers. Gjerloev and coworkers showed examples of classical substorms in which at the time of substorm onset the AL contributing station jumped from a location near the dawn terminator to the premidnight location of the onset seen in satellite images. Gjerloev and coworkers also noted, however, that the difference in time between the jump and the image-determined onset time rarely exceeded a few minutes. Thus, the existence of an onset and its occurrence time is not affected by the difficulty in determining its location in MLT, but

Table 2
Numbers of Magnetic Perturbation Events (MPEs) Observed at Each Station With Derivative Amplitude |dB/dt| ≥6 nT/s in Any Component, as a Function of Δt, the Time Delay After the Most Recent Prior Substorm Onset

Station	MLAT	Δt ≤30 min #	Δt ≤30 min %	30 < Δt < 60 min #	30 < Δt < 60 min %	Δt ≥60 min #	Δt ≥60 min %	All #
RBY	75.2°	50	60	21	25	13	15	84
CDR	72.7°	112	68	32	20	21	12	165
IQA	71.4°	118	66	29	16	32	18	179
SALU	70.7°	186	66	47	17	48	17	281
KJPK	64.7°	77	63	20	16	25	20	122

because satellite imager data were not available during 2015 and 2017, it is impossible to accurately determine the MLT location of all of the relevant substorm onsets.

4. MPE Occurrences as a Function of Derivative Amplitude

Figure 3 shows the distribution of occurrences of MPEs as a function of derivative amplitude at all five stations and in all three time delay categories. Different symbols are used to designate events based on the time of MPE occurrence after the closest prior substorm onset: blue circles for Δt ≤30 min, green squares for Δt between 30 and 60 min, and red triangles for Δt ≥60 min. The number of MPEs in each 1 nT/s bin was largest at the lowest amplitudes at all stations, but exhibited a long tail. There was no clear latitudinal trend.

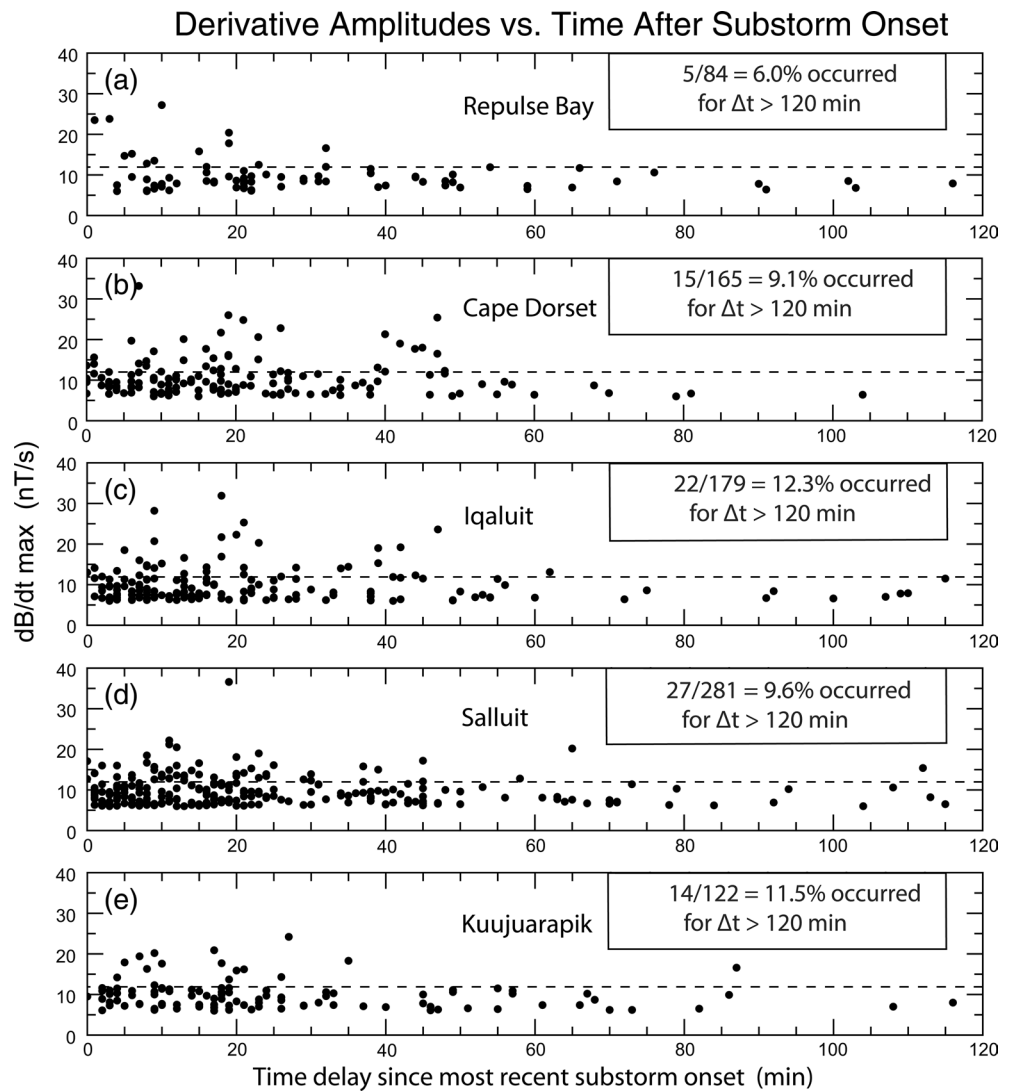**Figure 2.** Plot of the amplitude of the maximum |d*B*/d*t*| value in any nighttime MPE component observed at each station as a function of its delay after the most recent substorm onset: (a) Repulse Bay, (b) Cape Dorset, (c) Iqaluit, (d) Salluit, and (e) Kuujuarapik. Only events with maximum derivative amplitude ≥6 nT/s are shown. The horizontal dotted line indicates an amplitude of 12 nT/s. MPE, Magnetic Perturbation Event.
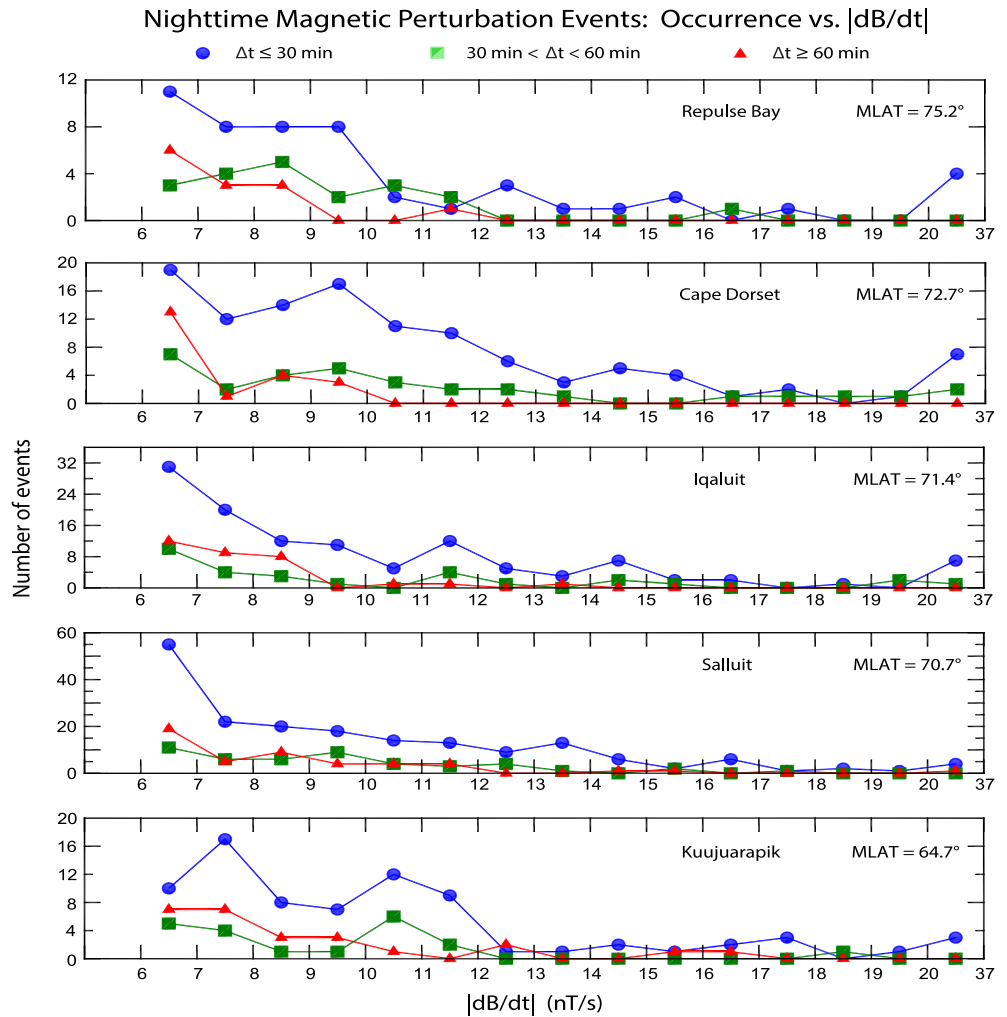
Figure 3. Plots of the number of occurrences of ≥6 nT/s nighttime MPEs observed at Repulse Bay, Cape Dorset, Iqaluit, Salluit, and Kuujuarapik as a function of the maximum derivative amplitude, sorted by each station's magnetic latitude. Events are color-coded based on time of occurrence after the closest prior substorm onset: Δt ≤30 min (blue circles), 30 < Δt < 60 min (green squares), and Δt ≥60 min (red triangles). The last interval at the right includes all events with amplitude >20 nT/s. Note that the vertical scales are different in each panel. MPEs, Magnetic Perturbation Events.

5. Latitudinal Distributions of Occurrences and Amplitudes Versus MLT, SYM/H, and SME

In this section, we show plots for each of the five stations of the numbers of occurrences and amplitudes of MPE events as functions of three variables: magnetic local time (MLT), the SYM/H index, and the SME index.

Over the range of magnetic latitudes covered in this study (from 65° to 75° MLAT) all ≥6 nT/s perturbation events fell into the local time range from 17 to 07 MLT. Figure 4a shows the number of occurrences of these MPEs at each station grouped in 1-h MLT bins and sorted by magnetic latitude. Different symbols are used to designate events based on the time of MPE occurrence after the closest prior substorm onset: plus signs for Δt ≤30 min, open squares for Δt between 30 and 60 min, and open triangles for Δt ≥60 min. Two populations are evident in this figure: a broad distribution extending from dusk to shortly after midnight (17–1 MLT) that appears at all latitudes shown, and a distribution in the postmidnight to dawn sector (2–7 MLT) that is prominent only at the lower latitude stations. This difference in latitudinal distribution, which is consistent with observations of large ionospheric equivalent current perturbations by Juusola et al. (2015),
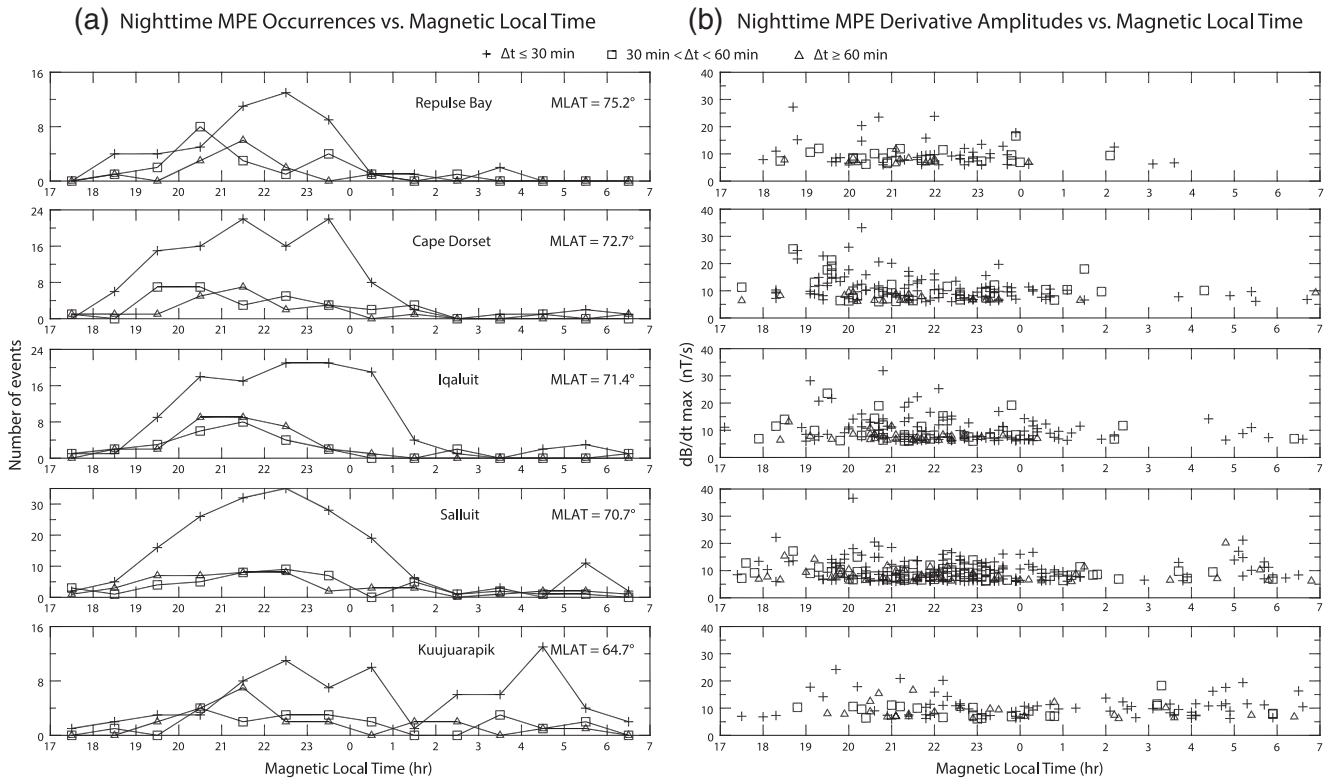
(a) Nighttime MPE Occurrences vs. Magnetic Local Time   (b) Nighttime MPE Derivative Amplitudes vs. Magnetic Local Time

Figure 4. Panel (a) shows the number of occurrences of ≥6 nT/s nighttime MPEs observed at Repulse Bay, Cape Dorset, Iqaluit, Salluit, and Kuujuarapik in 1-h bins of MLT from 17 to 07 h, sorted by each station's magnetic latitude. Panel (b) shows the distribution of MPE derivative amplitude at these same stations. Different symbols are used to designate events based on the time of MPE occurrence after the closest prior substorm onset: plus signs for Δt ≤30 min, open squares for Δt between 30 and 60 min, and open triangles for Δt ≥60 min. MLT, magnetic local time; MPEs, Magnetic Perturbation Events.

Table 3
Distribution of "Pre- and Postmidnight" ≥6 nT/s Magnetic Perturbation Events (MPEs) at Each Station as a Function of Time Between the Most Recent Substorm Onset and Event Occurrence. "Premidnight" MPEs Include Those Observed Between 1700 and 0100 MLT, and "Postmidnight" Events Those Between 0200 and 0700 MLT

	RBY		CDR		IQA		SALU		KJPK	
Station	#	%	#	%	#	%	#	%	#	%
"Premidnight"										
t ≤30 min	47	59	105	70	105	64	145	66	43	56
30–60 min	19	24	28	19	26	16	38	17	15	19
t ≥60 min	13	16	18	12	32	20	39	18	19	25
Sum	79		151		163		221		77	
Combined: t ≤30 min: 64%, 30–60 min: 18%, t ≥60 min:17%										
"Postmidnight"										
t ≤30 min	3	75	5	56	7	70	18	56	31	74
30–60 min	1	25	3	33	3	30	7	22	5	125
t ≥60 min	0	0	1	11	0	0	7	22	6	140
Sum	4		9		10		32		42	
Combined: t ≤30 min: 66%, 30–60 min: 20%, t ≥60 min: 14%										

appears to reflect the latitudinal dependence of the auroral electrojet, which is located at higher latitudes premidnight and lower latitudes postmidnight. As will be shown in later parts of this study, the properties of these two populations also differed somewhat in their association with different geomagnetic conditions.

Consistent with the distribution of occurrences shown in Table 2 and Figure 2, Figure 4a shows that the MPEs that occurred within 30 min of the most recent substorm onset (shown with a plus sign) were the dominant category in nearly all MLT bins at each station. The local time trends for MPEs shown with squares and triangles were similar to those for MPEs shown with plus signs for the four most poleward stations, with a broad distribution gradually rising from ∼17 to 18 h MLT to a broad premidnight peak before gradually falling to ∼1–2 h MLT, and with very few events occurring at later MLT. At KJPK, the premidnight distribution of events shown with plus signs was somewhat narrower in time and shifted toward slightly later MLT, and a second postmidnight peak (with similar peak occurrences) appeared between 2–3 and 6 h MLT. In contrast, the distributions for events shown with squares and triangles were flat across the entire MLT range shown (but with fewer occurrences).

Figure 4b shows that large-amplitude MPEs occurred at all five stations between 1800 and 2300 h MLT, but derivatives with amplitude at or above 15 nT/s also appeared after 0300 h MLT at both SALU and KJPK. Table 3 shows an analysis of the distribution of these events as a function of time
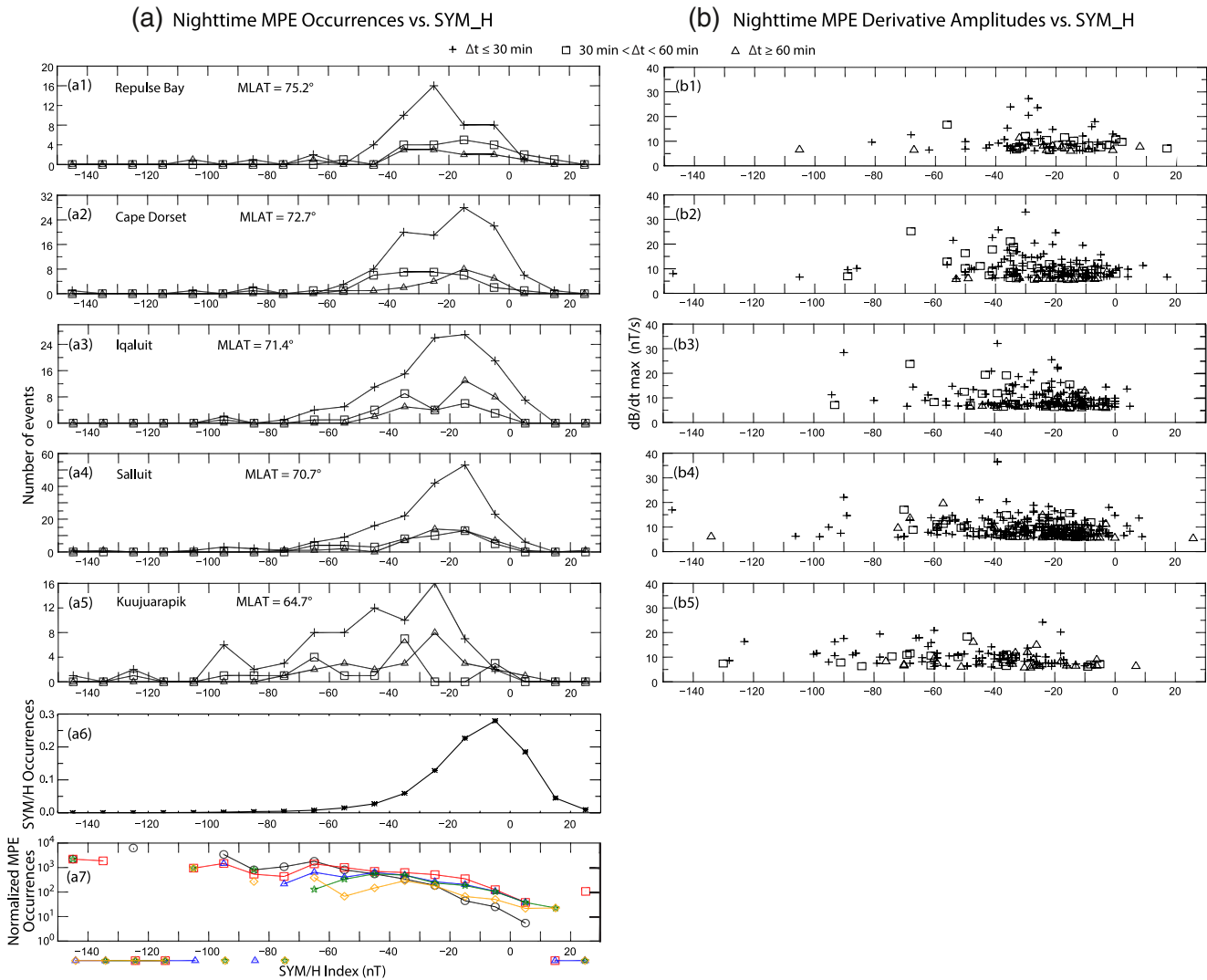
Figure 5. Panels (a1–a5) and (b1–b5) are plots of ≥6 nT/s nighttime MPE occurrences and amplitudes as in Figure 4, but as a function of the SYM/H index. Panel (a6) shows the fractional distribution of SYM/H values in 10-nT bins from −150 to +30 nT during the full years 2015 and 2017. Panel (a7) is a logarithmic plot of the distribution of all nighttime MPE occurrences at each station, normalized by the fractional distribution of SYM/H values. RBY: orange diamonds, CDR: green stars, IQA: blue triangles, SALU: red squares, and KJPK: black circles. Symbols for bins with zero events are shown below the horizontal axis. MPE, Magnetic Perturbation Event.

delay when separated into "pre- and postmidnight" occurrences. In order to clearly separate these categories, "premidnight" events were chosen to include those observed between 1700 and 0100 MLT, and "postmidnight" events those between 0200 and 0700 MLT. The time delay distributions were similar for "pre-" and "postmidnight" events at all five stations.

Panels (a1–a5) of Figure 5a show plots similar to those in Figure 4a of MPE occurrences as a function of the SYM/H index, which ranged from ∼−150 to +30 nT during these events. Panel (a6) shows the fractional distribution of SYM/H index values in 10-nT bins from −150 to +30 nT during all of 2015 and 2017. This distribution was above 0.1 only between −30 and +10 nT, peaked between −10 and 0 nT, and dropped off rapidly for values beyond that range. At all five stations, the MPE occurrence distributions peaked between −30 and −10 nT, thus for SYM/H values between 10 and 20 nT more negative than the peak of the SYM/H distribution. The tails of the MPE distributions at more negative SYM/H values increased from the highest to the lowest latitude station (KJPK). This most likely reflects the equatorward expansion of the auroral oval during geomagnetic storms. The occurrence distributions for the three time delay categories were roughly similar to each other at each station.

Panel (a7) of Figure 5a shows a color-coded logarithmic plot of the normalized distribution of all MPEs at each station (the sum of events in all three categories in each bin divided by the fractional distribution of SYM/H values in that bin). In contrast to the actual MPE occurrence rate, this normalized distribution shows that at each of these stations MPEs were factors of ~10 to over 100 more likely to occur under relatively rare storm-time conditions (large negative SYM/H) than under the much more common non-storm-time conditions.

Figure 5b shows that the SYM/H range corresponding to the largest derivative amplitudes (>20 nT/s) occurred for values between −40 and −20 nT at RBY and expanded toward lower SYM/H values at CDR and IQA. Even though many more MPEs occurred at SALU and KJPK than at the three higher latitude stations during storm conditions (with values of SYM/H less than −60 nT), the largest storm-time MPEs at these stations were no larger than MPEs during nonstorm conditions, even near 65° MLAT. However, more events at SALU and KJPK occurred with lower amplitude during nonstorm conditions.

At all five stations >6 nT/s perturbation events occurred over a wide range of SME values, as shown in panels (a1–a5) of Figure 6a, but very few events occurred at any station for SME < 200 nT. Panel (a6) shows the fractional distribution of SME values in 100-nT bins from 0 to 1,500 nT during all of 2015 and 2017. The fraction of SME events between 0 and 100 nT was slightly higher than the fraction between 100 and 200 nT, but the distribution dropped off rapidly for values above 200 nT. At the four highest latitude stations, a large majority of events in each of the three time delay categories occurred for SME values between 200 and 900 nT. This SME range also held at the lowest latitude station (KJPK) for the Δt >60 min category, but most of the events in the Δt ≤30 min category were associated with SME values >800 nT. However, fewer events occurred for high SME at KJPK (64.7° MLAT) than at SALU (70.7° MLAT)—note the differing vertical scales. Comparison of the MPE distributions at each station with the SME distribution shown in panel (a6) shows clearly that at least moderate levels of SME are associated with all MPEs.

Panel (a7) of Figure 6a shows a color-coded logarithmic plot of the normalized distribution of all MPEs at each station (the sum of events in all three categories in each bin divided by the fractional distribution of SME values in that bin). In contrast to the actual MPE occurrence rate, this normalized distribution shows that at each of these stations MPEs were factors of ~5–30 more likely to occur under high SME conditions than under the much more common moderate SME conditions.

Figure 6b shows that there was a modest correlation between the amplitude of the largest derivatives and the SME index only over the SME range between 200 and 600 nT at all five stations; the distribution of amplitudes was nearly flat for SME >600 nT at all stations. Most events at all SME values and all three time ranges were below 12 nT/s. Only 4 of the 831 total events occurred when SME exceeded 2000 nT.

6. Event Occurrence in Relation to Substorms and Magnetotail Dipolarizations

In this section, we address three questions: (1) What percentages of substorms are associated with a large nighttime MPE? (2) How important are multiple-onset substorms for large-amplitude MPEs? and (3) to what extent are nighttime MPEs associated or not with dipolarizations observed at geosynchronous orbit?

6.1. Percentages of Substorms Associated With Large Nighttime MPEs

Figure 2 and Table 2 have shown the numbers and percentages of MPEs that are associated with substorm onsets within given ranges of time delays. We now address the reverse association: in what percentage of substorm onsets does an MPE occur within one hour?

In order to address this question, we compared the number of observed MPEs to the number of substorm onsets listed in the SuperMAG onset database for 2015 and 2017. Roughly 80% of the MPE events at the four northernmost stations occurred between 1900 and 0100 MLT (Figure 4), and most (~60%) of the MPEs observed at all five stations occurred from 0 to 30 min after the most recent substorm onset (Figure 2). We thus wish to determine the number of substorm onsets that might correspond to MPE events between 1830 and 0100 MLT. Figure 2 of Frey et al. (2004) shows the distribution of substorm onsets in the MLT range from 16 to 04 h determined by using data from the Far Ultra-Violet imager on the IMAGE satellite obtained
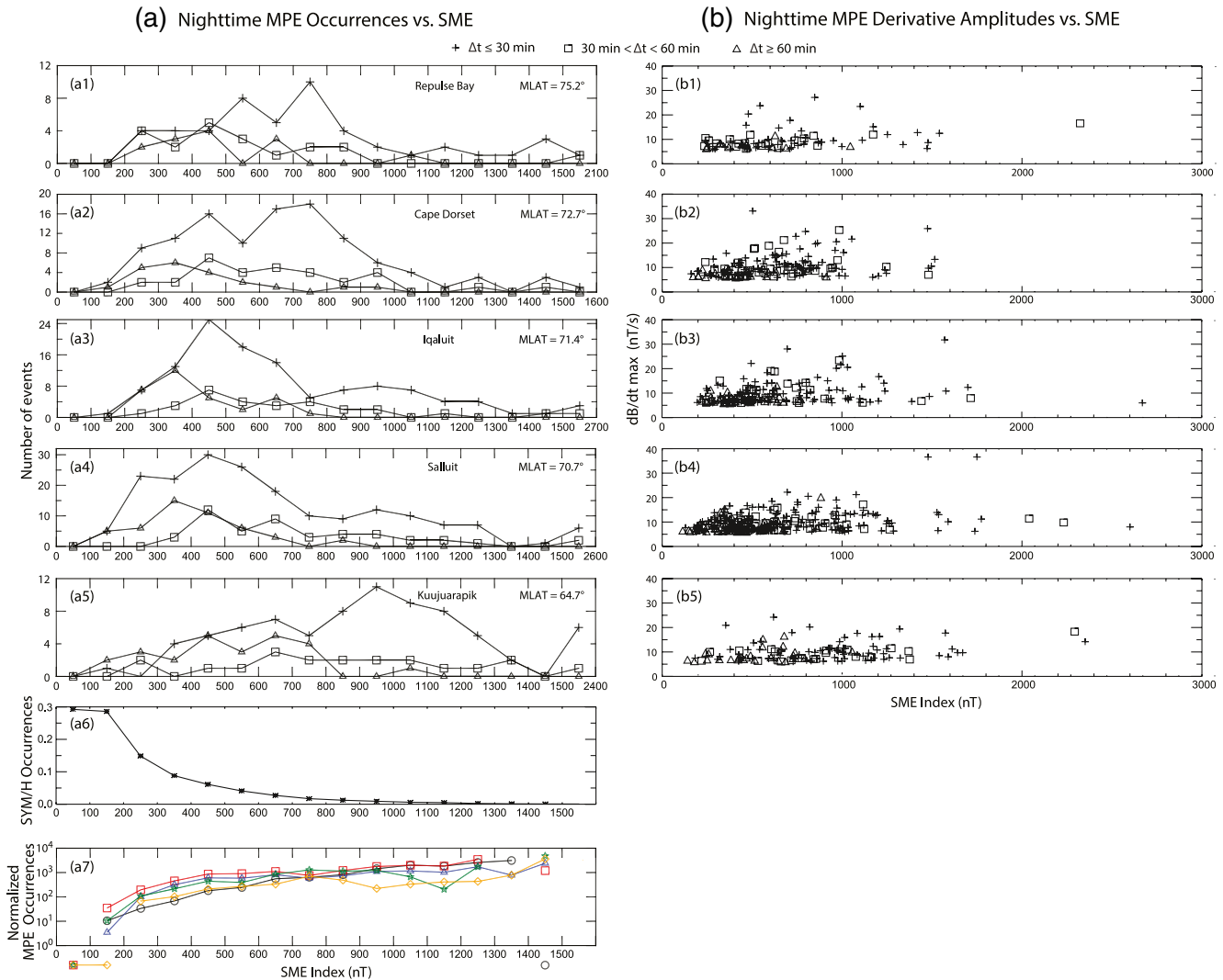
Figure 6. Panels (a1–a5) and (b1–b5) are plots of ≥6 nT/s nighttime MPE occurrences and amplitudes as in Figure 4, but as a function of the SME index. In Figure 6a, the events at each station are binned in steps of 100 nT, except for the rightmost bin, which includes all events with SME between 1,500 and the maximum value shown in the horizontal legend for each station. The horizontal axis in panels (b1–b5) covers the full range of SME values recorded during MPEs in this study. Panel (a6) shows the fractional distribution of SME values in 100-nT bins from 0 to 1,500 nT during the full years 2015 and 2017. Panel (a7) is a logarithmic plot of the distribution of all nighttime MPE occurrences at each station from 0 to 1,500 nT, normalized by the fractional distribution of SYM/H values. RBY: orange diamonds, CDR: green stars, IQA: blue triangles, SALU: red squares, and KJPK: black circles. Symbols for bins with zero events are shown below the horizontal axis. MPE, Magnetic Perturbation Event.

between May 19, 2000 and December 31, 2002. No comparable imager data were available during 2015 and 2017. Substorm onset occurrences in the Frey et al. (2004) study peaked at 23.0 MLT and fell off sharply in both directions. The premidnight part of this distribution is consistent with the distribution of MPEs shown at all stations in Figure 4 except KJPK. However, during magnetic storms the onset location has a wider spread, and thus a postmidnight tail in the onset distribution can be associated with onsets that occur during an expanded auroral oval, more consistent with the MPE distribution observed at KJPK.

At the CDR and SALU stations, located in magnetic longitude near the center of the five stations, the 1830 to 0100 MLT range corresponds to a time window from 2325 to 0555 UT. The SuperMAG substorm onset data base indicated that during 2015 and 2017 combined, 932 of a total of 4,031 onsets occurred during this UT time window.

Columns 2–4 of Table 4 show the number of MPE events at each station that occurred within this UT time window as a function of their time delays (0–30, 30–60, and 0–60 min) after the most recent substorm onset.

Table 4
The Numbers of ≥6 nT/s Magnetic Perturbation Events (MPEs) Observed at Five Stations During 2015 and 2017 Between 2325 and 0555 UT as a Function of Their Time Delays (0–30, 30–60, and 0–60 min) After the Most Recent Substorm Onset (Columns 2–4), These Numbers as Percentages of the Estimated Number of Substorm Onsets (Columns 5–7), and the Estimated Percentages of Substorm Onsets After Which No MPE Occurred Within 60 min After Onset (Column 8)

Station	Number of events			% following a substorm onset			SS onset % not
	0–30 min	30–60 min	0–60 min	0–30 min	30–60 min	0–60 min	Related to MPEs
RBY	50	21	71	5.4	2.3	7.6	92.4
CDR	112	32	144	12.0	3.4	15.4	84.6
IQA	118	29	147	12.7	3.1	15.8	84.2
SALU	186	47	233	20.0	5.0	25.0	75.0
KJPK	77	20	97	8.3	2.1	10.4	89.6

Columns 5–7 show the estimated percentage of events following a documented substorm onset within these time delays, calculated by dividing the number of events in columns 2–4 by 932. Column 7 shows that the percentage of MPEs per substorm onset that occurred within 60 min after an identified substorm varied from 7.6% to 25.0%. Column 8 shows the reverse occurrence: the estimated percentage of substorm onsets after which no MPE occurred within 60 min after onset. The percentages in this column ranged from 75% to 92%, indicating that most substorms were not associated with large amplitude MPEs. The percentages at CDR, IQA, and SALU were near the lower end of this range, and those at RBY and KJPK at the higher end. We note the roughly inverse correlation between these percentages and the number of MPE events observed at each station (Table 2). This dependence on MLAT may reflect the limited spatial extent of large MPEs, such that a station farther away from the statistical auroral oval is more likely to detect an MPE with lower amplitude, and thus in many cases, one below our selection threshold of 6 nT/s.

6.2. The Importance of Multiple Prior Substorm Onsets for Large Nighttime MPEs

We also considered the effect of multiple prior substorm onsets (or intensifications) separately for MPEs in the two populations shown in Figure 4a: the "premidnight" population observed between 1700 and 0100 MLT, and the "postmidnight" population observed between 0200 and 0700 MLT. Table 5 shows the number of >6 nT/s MPEs observed during 2015 and 2017 as a function of the number of substorm onsets that

Table 5
The Number of ≥6 nT/s Magnetic Perturbation Events (MPEs) Observed During 2015 and 2017 at the Three Lowest Latitude Stations as a Function of the Number of Substorm Onsets That Occurred Within 2 h Prior to the MPE

Station	Number of onsets							
	0	1	2	3	4	5	6	Total
IQA								
1700-0100 MLT	22	82	40	15	4	0	0	163
0200-0700 MLT	0	2	2	4	2	0	0	10
SALU								
1700-0100 MLT	21	115	61	20	4	0	0	221
0200-0700 MLT	4	5	7	10	6	0	0	32
KJPK								
1700-0100 MLT	13	28	22	10	3	1	0	77
0200-0700 MLT	1	5	16	10	8	0	2	42
Full year probability distribution for 2015 and 2017 combined	69.4	19.3	7.9	2.4	0.8	0.2	0.01	100

Notes. Events at IQA, SALU, and KJPK are separated into two local time ranges: from 1700 to 0100 MLT and 0200–0700 MLT. The last line of the table shows the probability distribution of the number of onsets during 2-h UT intervals from 00-02 to 22–24 UT during full years 2015 and 2017.
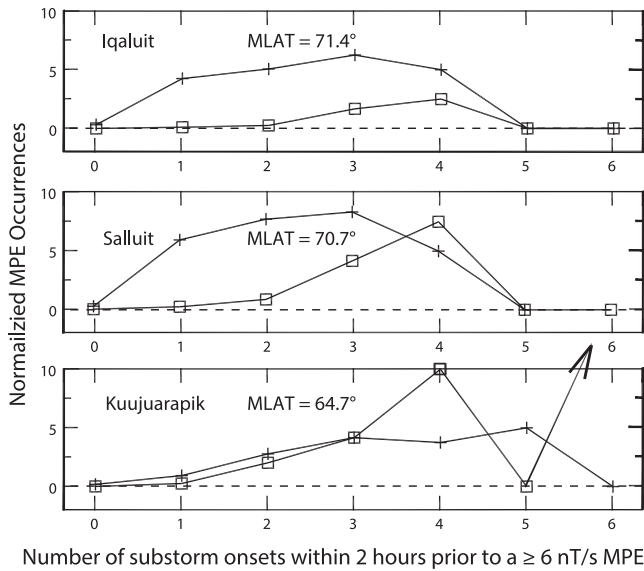
Figure 7. Plot of the normalized occurrences of MPEs observed during 2015 and 2017 as a function of the number of substorm onsets that occurred within 2 h prior to the MPE, at IQA, SALU, and KJPK. Plus signs and open squares indicate "pre-" and "postmidnight" events, respectively. MPE, Magnetic Perturbation Event.

occurred within 2 h UT prior to the MPE. Only the three lowest latitude stations are included in this table because of the very small number of "postmidnight" events at the two higher latitude stations. The bottom row of Table 5 shows the probability distribution of the number of substorm onsets during 2-h UT intervals from 00–02 to 22–24 UT during full years 2015 and 2017. This background distribution peaked at 0 prior onsets, and dropped by successive factors of ∼2 to ∼4 from 0 to up to five prior onsets.

Figure 7 shows the normalized distribution of these MPEs (the number of MPEs in each category divided by the substorm occurrence percentage of that category). Although 22 and 21 "premidnight" MPEs occurred at IQA and SALU respectively when there were no substorm onsets during the prior 2 h (category 0), their normalized occurrence values were 0.32 and 0.30, considerably lower than the normalized values in categories 1–4. The normalized "premidnight" category 0 value at KJPK was even lower (0.17) and its values rose more slowly and peaked in categories 3–5. The "postmidnight" normalized distributions at all three stations, however, rose monotonically from even lower category 0 values (0, 0.04, and 0.01) to their peak values in category 4. Table 6 shows the results of applying Pearson's Chi-square test to the data in Table 5, after reducing the number of prior substorm categories to 3: after 0, 1, and ≥2 onsets within 2 h, respectively, to test the hypothesis that there is a significant difference in the number of >6 nT/s MPEs in each prior substorm category between "premidnight" and "postmidnight" MPEs. The p values of << 0.05 confirm the hypothesis: there is a much stronger relation between multiple substorms and subsequent MPEs in the "postmidnight" sector than in the "premidnight" sector.

Table 7 provides additional information on the relation between MPE onset and the level of magnetic disturbance (as represented by the SME index) following multiple substorms. This table shows for both "pre-" and "postmidnight" sectors and for IQA, SALU, and KJPK (a) the total number of MPEs observed as a function of the number of substorm onsets during the 2 h prior to the MPE, (b) the number of MPEs simultaneous with very intense magnetic disturbances (SME ≥1,000 nT), and (c) the percentage of these MPEs compared to the total number of MPEs observed in each onset bin. At all three stations and for both "premidnight" and "postmidnight" events, (1) no MPEs occurred in the first bin (following a 2-h period after 0 substorms) and very few in the second bin (following 1 substorm), (2) most MPEs simultaneous with SME values ≥1,000 nT occurred after two-hour intervals containing from 2 to 4 substorm onsets, and (3) the percentage distribution of "premidnight" MPEs simultaneous with SME values ≥1,000 nT increased greatly as the number of prior substorm onsets increased from 1 to 4, but was more nearly flat for "postmidnight" events. The overall fractions of "premidnight" MPEs associated with SME values ≥1,000 nT were 9.2% at IQA, 8.5% at SALU, and 19.4% at KJPK. The corresponding "postmidnight" fractions were much larger: 70%, 44%, and 52%, respectively.

The SME index is well correlated with auroral power (Newell & Gjerloev, 2011a). In general, the relationship among discrete precipitation, ionospheric conductance, and upward FAC density is instantaneous. In contrast, diffuse precipitation has a certain time lag; particles are injected and then later forced to precipitate into the ionosphere. The associated enhancement of ionospheric conductance lasts longer, which is favorable for more tail current to short-circuit through the ionosphere at subsequent substorms. As a result, SME may increase following multiple particle injections closely spaced in time more than it would without continuing activity, independently of the intensity of any individual substorm.

Table 6
Application of Pearson's Chi-Square Test With 2 degrees of Freedom to the Number of "Pre-" and "Postmidnight" Magnetic Perturbation Event (MPE) Occurrences as a Function of the Number of Prior Substorm Onsets Within 2 h

MLT range	17–1	2–7	17–1	2–7	17–1	2–7
Station	IQA		SALU		KJPK	
0 onsets	22	0	21	4	13	1
1 onset	82	2	115	5	28	5
≥2 onsets	59	8	85	23	36	36
χ^2	7.80		15.378		17.54	
p-value	0.02		0.00046		0.00016	

Table 7
*The Number and Normalized Percentage of "Pre- and Postmidnight"
≥6 nT/s Magnetic Perturbation Events (MPEs) With SME ≥1,000 nT
Observed at IQA, SALU, and KJPK During 2015 and 2017, as a Function
of the Number of Substorm Onsets That Occurred Within 2 h Prior to the
MPE*

	Number of onsets						
Station	0	1	2	3	4	5	6
1700-0100 MLT							
IQA							
Total MPEs	220	82	40	15	4	0	0
# SME ≥1,000 nT	0	2	6	5	3	–	–
% SME ≥1,000 nT	0	2	15	33	75	–	–
SALU							
Total MPEs	21	115	61	20	4	0	0
# SME ≥1,000 nT	0	7	6	5	2	0	–
% SME ≥1,000 nT	0	6	10	24	60	0	–
KJPK							
Total MPEs	13	28	22	10	3	1	0
# SME ≥1,000 nT	0	2	5	3	2	0	–
% SME ≥1,000 nT	0	7	23	30	67	0	–
0200-0700 MLT							
IQA							
Total MPEs	0	2	2	4	2	0	0
# SME ≥1,000 nT	0	0	2	3	2	0	–
% SME ≥1,000 nT	0	0	100	75	100	0	–
SALU							
Total MPEs	4	5	7	10	6	0	0
# SME ≥1,000 nT	0	0	2	6	5	0	–
% SME ≥1,000 nT	0	0	29	60	83	0	–
KJPK							
Total MPEs	1	5	16	10	8	0	2
# SME ≥1,000 nT	0	1	10	6	4	0	2
% SME ≥1,000 nT	0	20	63	60	50	0	100

These differing patterns again indicate that intervals of large SME (or AE) index values are poorly correlated with intense "premidnight" dB/dt values but are better correlated for "postmidnight" events.

6.3. Relation of Large Nighttime MPEs to Dipolarizations at Synchronous Orbit

In each of the three case studies of MPEs in paper 2, which occurred within 30 min of a substorm onset, rapid increases of from 15 to 30 nT in the B_z component of the magnetic field (dipolarizations) at GOES 13 coincided with an MPE to within a few minutes. In this section, we present data from two stations: RBY, the station at the highest magnetic latitude, and KJPK, the station at the lowest magnetic latitude and located closest to the magnetic footpoint of GOES 13. Figure 8 presents a comparison of the B_z perturbations observed at GOES 13 within 45 min prior to each of the MPEs observed at RBY and KJPK during 2015 and 2017, grouped in two categories: MPEs with time delays ≥60 min and ≤30 min after the most recent substorm onset. Of the events with time delays ≥60 min, GOES data were available for 12 of the 13 MPEs at RBY and for all 25 of the MPEs at KJPK. Of the events with time delays ≤30 min, GOES data were available for 49 of the 50 MPEs at RBY and all 77 of the MPEs at KJPK. At RBY 3 of 12 and 4 of 49 GOES 13 B_z perturbations, respectively, were negative and are not shown in Figure 8; the corresponding numbers at KJPK were 0 of 25 and 2 of 77, respectively. Figure 8 shows that at both stations the amplitude distribution of the perturbations did not extend to as large values for the Δt ≥60 min MPE population as for the ≤30 min MPE population.

Some of the smaller GOES 13 B_z perturbations, and especially those in the Δt ≥60 min category, were associated with brief (few minutes) transient pulses rather than step functions (dipolarizations). It is difficult to discern whether such pulses arise from spatial or temporal effects. If spatial, GOES 13 may have been rather distant in MLT from the center of a more large-scale dipolarization. If temporal, the perturbation may have been associated with a bursty bulk flow, dipolarization front, and/or pseudobreakup (e.g., Palin et al., 2015). Further analysis of the features of the GOES 13 data set during these MPE events is certainly warranted, but is beyond the scope of this paper.

7. Summary of Observations

This study has described the distributions of ≥6 nT/s nighttime MPEs as functions of several physical parameters and geomagnetic indices, and has identified two different populations on the basis of differences in both MLT and dependence on magnetic activity levels. The first two of the MPE characteristics listed in this section confirm and extend the observations in previous reports as detailed below, but others appear to provide new information.

1. Distributions of MPEs as functions of the time delay after a substorm onset were presented by Viljanen et al. (2006), using data from Longyearbyen, Sodankylä, and Nurmijarvi and in paper 2, using data from Repulse Bay. Both studies found that these distributions had long tails. This study confirms and quantifies the occurrence of these long tails: Although many of the most intense MPEs at each station occurred within 30 min of a substorm onset, from 13% to 20% of the MPEs at each station occurred later than 1 h after the most recent substorm onset, and from 6% to 12% later than 2 h. The strongest MPEs at all five stations most often occurred within 60 min of a substorm onset, but the amplitudes of most events were below 12 nT/s at all delay times
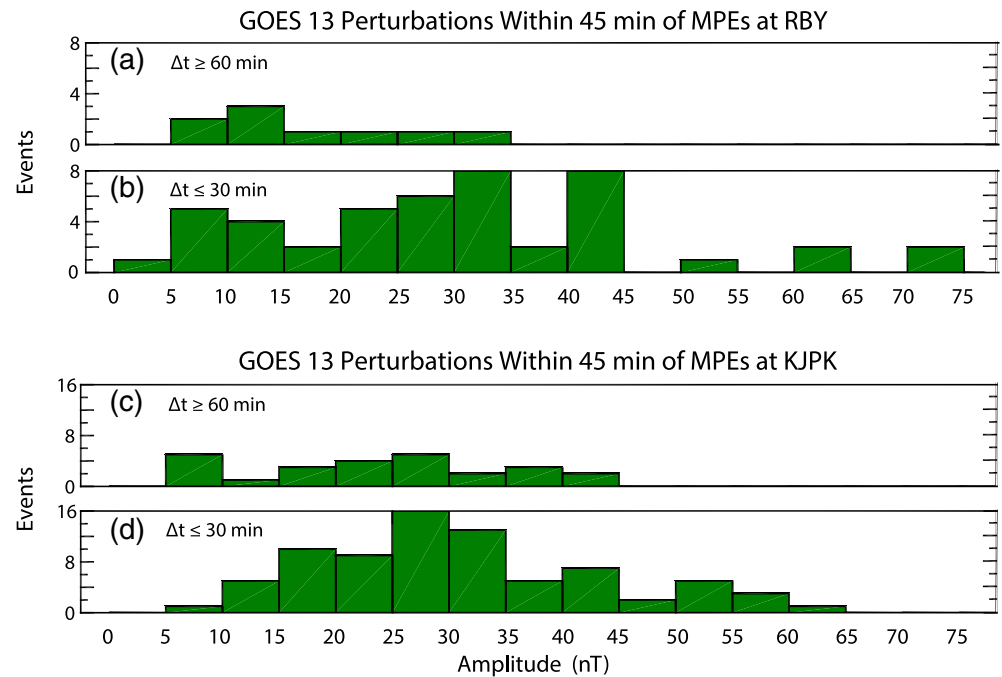
Figure 8. Plots of the number of GOES 13 perturbations occurring within 45 min prior to MPEs observed at RBY and KJPK, as a function of amplitude. Panels (a and c) show the distribution of amplitudes for MPEs occurring ≥60 min after the most recent substorm onset, and panels (b and d) show the distribution for MPEs occurring ≤30 min after the most recent substorm onset. MPEs, Magnetic Perturbation Events.

2. A broad distribution of nighttime MPEs appeared at all five stations between 1700 and 0100 MLT, and a narrower distribution appeared at the lower latitude stations between 0200 and 0700 MLT. This is consistent with earlier studies by Viljanen et al. (2001), Viljanen and Tanskanen (2011), Juusola et al. (2015), and most recently by Vorobev et al. (2019) that showed both "pre-" and "postmidnight" occurrence peaks. Our study has shown that MPEs occurring within 30 min of a substorm onset dominated in nearly all MLT bins at each station

3. The number of MPEs decreased roughly linearly with amplitude at all five stations and in all three time delay categories, with no clear latitudinal trend

4. The probability of MPE occurrence for a given range of SYM/H was higher for more negative values, as shown in panel (a7) of Figure 5, but at all five stations the total number of MPE occurrences peaked during quiet conditions (SYM/H between −20 and −30 nT). At all but the lowest latitude station nearly all MPEs occurred for SYM/H values between −60 and +10 nT. More MPEs occurred at KJPK during times SYM/H was < −40 nT, reflecting the equatorward expansion of the auroral oval during geomagnetic storms. We would thus expect that stations at subauroral latitudes would observe proportionally more MPEs at times corresponding to more negative SYM/H values.

5. The SYM/H range corresponding to the largest MPE amplitudes was between −40 and −20 nT at RBY and expanded toward lower SYM/H values with lower latitudes, but there was little or no correlation between the largest MPE amplitudes and SYM/H values at the two lowest latitude stations (SALU and KJPK). Storm-time MPEs were no more likely to have extreme derivative values than MPEs during non-storm conditions, even near 65° MLAT (KJPK)

6. MPE occurrences at all five stations were spread over a wide range of SME values above ∼200 nT. At the four highest latitude stations, a large majority of MPEs in each of the three time delay categories occurred for SME values between 200 and 900 nT. Only at KJPK was the distribution dominated by events with SME >800 nT, and that only for events within 30 min of substorm onset. There was a modest correlation between the amplitude of the largest MPEs and the SME index over the SME range from ∼200 to ∼600 nT, but the distribution of amplitudes was nearly flat for SME > 600 nT. The amplitude of most MPEs at all SME values and in all three time categories was below 12 nT/s

7. We compared the peak range of the distributions of substorm onsets and MPE onsets during 2015 and 2017 in order to estimate the percentages of substorm onsets after which no MPE occurred within 60 min. These ranged from 75% to 92% at the five stations, indicating that most substorms were not associated with ≥6 nT/s MPEs

8. The importance of multiple prior substorm onsets (within 2 h) for MPE occurrence was different for "pre-" and "postmidnight" MPEs. In the 1700-0100 MLT sector, the distribution of MPEs peaked in the 1 prior substorm onset bin and fell off rapidly above 2; in the 0200–0700 MLT sector, the distribution of MPEs exhibited a broad maximum between 1 and 4 prior onset bins. When the distribution of MPEs was normalized by the number of onsets occurring within 2-h intervals, "premidnight" MPE occurrences exhibited a broad maximum between 1 and 5 onsets, while "postmidnight" MPE occurrences rose gradually to a sharp peak at 4 onsets. "Premidnight" MPEs exhibited a relatively flat distribution of median MPE amplitudes across all prior onset bins, while postmidnight MPEs exhibited a ∼50 % increase in median amplitudes from 1 to 4 prior onsets. The percentage of "premidnight" MPEs associated with highly disturbed geomagnetic conditions (SME ≥1,000 nT) varied inversely with the number of MPEs in each bin, whereas the percentage of "postmidnight" MPEs associated with SME ≥1,000 nT was largest in the same bins as the number of MPEs. The overall fractions of MPEs associated with SME ≥1,000 nT conditions ranged from 9.2% to 19.4% "premidnight" and 44%–70% "postmidnight"

9. At both RBY and KJPK, the amplitude of dipolarizations of the magnetic field at geosynchronous orbit observed by GOES 13 did not extend to as large values for the Δt ≥60 min MPE events as for the ≤30 min events. Many of the smaller dipolarizations at GOES 13 were associated with short-lived pulses rather than step functions

8. Discussion and Conclusions

Much of the literature on GICs has focused on magnetic storms. This is reasonable because many of the regions most threatened by GICs are located at magnetic latitudes equatorward of the nominal auroral oval, and only during major magnetic storms does the auroral oval expand significantly toward the equator. However, the extreme magnetic perturbations that cause nighttime GICs occur much more often at high latitudes, so that a study of MPEs at these latitudes provides a larger data base to characterize their occurrence and amplitude distributions. In particular, it provides information on their location in latitude and local time relative to auroral features, their temporal relation to substorms and nightside dipolarizations, and their occurrence and amplitude relative to indices of magnetic storm and substorm activity.

This study has shown that there was little or no correlation between the amplitude of the largest MPEs and increasingly disturbed conditions (as parameterized by more negative SYM/H values) at any of these stations, and that at the four highest latitude stations most MPEs occurred when SYM/H values were > −40 nT. Given that the overall distribution of SYM/H index values also peaked in this range, however, these data simply confirm that more MPEs occurred at higher latitudes when SYM/H values were nearer to 0, and that large MPEs were not restricted to times when SYM/H was strongly negative. However, when normalized by the overall distribution of SYM/H values the occurrence of MPEs was found to be from ∼10 to over 100 times more likely during disturbed intervals than during quiet intervals.

We have also found that only 60%–67% of the ≥6 nT/s MPEs we observed occurred within 30 min of the most recent substorm onset. A recent study by Freeman et al. (2019) found a similar result. They noted that in data from three stations in the United Kingdom over two solar cycles (only) 54%–56% of all extreme rate of change values occurred during substorm expansion or recovery phases.

The separation of nighttime MPEs into two populations in MLT, a "premidnight" one that appeared at all five stations and a "postmidnight" one that was prominent only at the two lowest latitude stations, has been noted in four previous papers cited above. This study has shown that the "postmidnight" MPE population occurred more often in conjunction with large SME values and after multiple substorm onsets than the "premidnight" MPEs.

Many observational studies have suggested possible links between MPEs and small-scale activity in the ionosphere and magnetotail. Paper 2 reviewed several earlier studies linking MPEs to westward traveling surges, polar boundary intensifications, auroral streamers, and small-scale nighttime magnetospheric

phenomena such as bursty bulk flows (Angelopoulos et al., 1992), their associated dipolarization fronts (Palin et al., 2015; Runov et al, 2009, 2011), and dipolarizing flux bundles (Gabrielse et al., 2014; Liu et al., 2015). However, many of these processes appear to be more relevant to the "premidnight" MPE population described here.

The local time range of the "postmidnight" MPE population matches that of omega bands (Syrjäsuo & Donovan, 2004), which were identified along with other auroral phenomena by Akasofu and Kimball (1964) and Akasofu (1974). Engebretson et al. (2020) reviewed many of the properties of omega bands, including the ionospheric currents associated with them, as part of a recent study of MPEs observed in conjugate hemispheres that included an interval of MPEs associated with omega bands, so these will not be repeated here. This study, however, pointed out that "postmidnight" MPEs exhibited even less temporal and spatial correlation between MPEs than "premidnight" MPEs, and suggested the possibility that the mesoscale mechanisms that produce MPEs in these two MLT ranges might be at least somewhat different. For example, Apatenkov et al. (2020) provided detailed observations in northern Scandinavia and northwest Russia of a very large GIC that was associated with an interval of omega bands. As a result of pointing out that the magnetic field created by ionospheric and magnetospheric currents may vary due to both temporal changes of current amplitudes and to motion of the current structures, they modeled this event using the sum of two basic current systems: a 1D linear current (mimicking the auroral electrojet) and a 2D vortex that passed eastward over the field of view of the ground magnetometers. Based on this model, they suggested that propagating nonexplosive and relatively long-lived structures might be responsible for large rapid magnetic field variations if their propagation speeds were sufficiently large.

The main implications of this study are (1) neither a magnetic storm nor a fully developed substorm is a necessary or sufficient condition for the occurrence of the extreme nighttime magnetic perturbation events that can cause GICs, and (2) the "pre-" and "postmidnight" populations of ≥6 nT/s MPEs and their consequent GICs differ not only in their occurrence in local time and latitude but also in their dependence on prior substorm activity and magnetospheric disturbance level.

Both this study and the several studies cited above thus point to localized processes in the nightside magnetosphere, several of which often occur during substorms but can also occur at other times and may take different configurations before and after midnight, as being responsible for generating these events. This underlines the importance of further studies of the associations between MPEs and these processes in order to fully understand their role in generating MPEs and the resulting GICs.

Data Availability Statement

Martin Connors; DTU Space, PI Dr. Thom R. Edwards and Anna Willer; PENGUIn; South Pole and Mc-Murdo Magnetometer, PIs Louis J. Lanzerotti and Allan T. Weatherwax; ICESTAR; RAPIDMAG; British Antarctic Survey; McMAC, PI Dr. Peter Chi; BGS, PI Dr. Susan Macmillan; Pushkov Institute of Terrestrial Magnetism, Ionosphere and Radio Wave Propagation (IZMIRAN); MFGI, PI B. Heilig; Institute of Geophysics, Polish Academy of Sciences, PI Anne Neska and Jan Reda; and University of L'Aquila, PI M. Vellante; BCMT, V. Lesur and A. Chambodut; Data obtained in cooperation with Geoscience Australia, PI Marina Costelloe; AALPIP, co-PIs Bob Clauer and Michael Hartinger; SuperMAG, Data obtained in cooperation with the Australian Bureau of Meteorology, PI Richard Marshall.

References

Akasofu, S.-I. (1974). A study of auroral displays photographed from the DMSP-2 satellite and from the Alaska meridian chain of stations. *Space Science Reviews*, *16*, 617–725.

Akasofu, S.-I., & Kimball, D. S. (1964). The dynamics of the aurora, 1, Instabilities of the aurora. *Journal of Atmospheric and Terrestrial Physics*, *26*, 205–211. https://doi.org/10.1016/0021-9169(64)90147-3

Angelopoulos, V., Baumjohann, W., Kennel, C. F., Coroniti, F. V., Kivelson, M. G., Pellat, R., et al. (1992). Bursty Bulk Flows in the inner central plasma sheet. *Journal of Geophysical Research*, *97*, 4027–4039. https://doi.org/10.1029/91JA02701

Apatenkov, S. V., Pilipenko, V. A., Gordeev, E. I., Viljanen, A., Juusola, L., Belakhovsky, V. B., et al. (2020). Auroral omega bands are a significant cause of large geomagnetically induced currents. *Geophysical Research Letters*, *47*, e2019GL086677. https://doi.org/10.1029/2019GL086677

Belakhovsky, V., Pilipenko, V., Engebretson, M., Sakharov, Y., & Selivanov, V. (2019). Impulsive disturbances of the geomagnetic field as a cause of induced currents of electric power lines. *Journal of Space Weather and Space Climate*, *9*, A18. https://doi.org/10.1051/swsc/2019015

Boteler, D. H., Pirjola, R. J., & Nevanlinna, H. (1998). The effects of geomagnetic disturbances on electrical systems at the Earth's surface. *Advances in Space Research*, *22*(1), 17–27. https://doi.org/10.1016/S0273-1177(97)01096-X

Carrington, R. C. (1860). Description of a singular appearance seen in the Sun on September 1, 1859. *Monthly Notices of the Royal Astronomical Society*, *20*, 13–15.

Connors, M., Schofield, I., Reiter, K., Chi, P. J., Rowe, K. M., & Russell, C. T. (2016). The AUTUMNX magnetometer meridian chain in Québec, Canada. *Earth, Planets and Space*, *68*. https://doi.org/10.1186/s40623-015-0354-4

Dimmock, A. P., Rosenqvist, L., Hall, J.-O., Viljanen, A., Yordanova, E., Honkonen, I., et al. (2019). The GIC and geomagnetic response over Fennoscandia to the 7-8 September 2017 geomagnetic storm. *Space Weather*, *17*, 989–1010. https://doi.org/10.1029/2018SW002132

Dimmock, A. P., Rosenqvist, L., Welling, D. T., Viljanen, A., Honkonen, I., Boynton, R. J., & Yordanova, E. (2020). On the regional variability of d*B*/d*t* and its significance to GIC. *Space Weather*, *18*, e2020SW002497. https://doi.org/10.1029/2020SW002497

Engebretson, M. J., Hughes, W. J., Alford, J. L., Zesta, E., Cahill, L. J., Jr., Arnoldy, R. L., & Reeves, G. D. (1995). Magnetometer array for cusp and cleft studies observations of the spatial extent of broadband ULF magnetic pulsations at cusp/cleft latitudes. *Journal of Geophysical Research*, *100*, 19371–19386. https://doi.org/10.1029/95JA00768

Engebretson, M. J., Kirkevold, K. R., Steinmetz, E. S., Pilipenko, V. A., Moldwin, M. B., McCuen, B. A., et al. (2020). Interhemispheric comparisons of large nighttime magnetic perturbation events relevant to GICs. *Journal of Geophysical Research: Space Physics*, *125*, e2020JA028128. https://doi.org/10.1029/2020JA028128

Engebretson, M. J., Pilipenko, V. A., Ahmed, L. Y., Posch, J. L., Steinmetz, E. S., Moldwin, M. B., et al. (2019). Nighttime magnetic perturbation events observed in Arctic Canada: 1. Survey and statistical analysis. *Journal of Geophysical Research: Space Physics*, *124*, 7442–7458. https://doi.org/10.1029/2019JA026794

Engebretson, M. J., Steinmetz, E. S., Posch, J. L., Pilipenko, V. A., Moldwin, M. B., Connors, M. G., et al. (2019). Nighttime magnetic perturbation events observed in Arctic Canada: 2. Multiple-instrument observations. *Journal of Geophysical Research: Space Physics*, *124*, 7459–7476. https://doi.org/10.1029/2019JA026797

Freeman, M. P., Forsyth, C., & Rae, I. J. (2019). The influence of substorms on extreme rates of change of the surface horizontal magnetic field in the United Kingdom. *Space Weather*, *17*, 827–844. https://doi.org/10.1029/2018SW002148

Frey, H. U., Mende, S. B., Angelopoulos, V., & Donovan, E. F. (2004). Substorm onset observations by IMAGE-FUV. *Journal of Geophysical Research*, *109*, A10304. https://doi.org/10.1029/2004JA010607

Gabrielse, C., Angelopoulos, V., Runov, A., & Turner, D. L. (2014). Statistical characteristics of particle injections throughout the equatorial magnetotail. *Journal of Geophysical Research: Space Physics*, *119*, 2512–2535. https://doi.org/10.1002/2013JA019638

Gjerloev, J. W., Hoffman, R. A., Friel, M. M., Frank, L. A., & Sigwarth, J. B. (2004). Substorm behavior of the auroral electrojet indices. *Annales Geophysicae*, *22*, 2135–2149. https://doi.org/10.5194/angeo-22-2135-2004

Juusola, L., Viljanen, A., van de Kamp, M., Tanskanen, E. I., Vanhamäki, H., Partamies, N., & Kauristie, K. (2015). High-latitude ionospheric equivalent currents during strong space storms: Regional perspective. *Space Weather*, *13*, 49–60. https://doi.org/10.1002/2014SW001139

Kamide, Y., & Kokubun, S. (1996). Two-component auroral electrojet: Importance for substorm studies. *Journal of Geophysical Research*, *101*(13), 027–13. https://doi.org/10.1029/96JA00142

Kappenman, J. G. (2005). An overview of the impulsive geomagnetic field disturbances and power grid impacts associated with the violent sun-earth connection events of 29–31 October 2003 and a comparative evaluation with other contemporary storms. *Space Weather*, *3*, S08C01. https://doi.org/10.1029/2004SW000128

Knipp, D. J. (2015). Synthesis of geomagnetically induced currents: Commentary and research. *Space Weather*, *13*, 727–729. https://doi.org/10.1002/2015SW001317

Liu, J., Angelopoulos, V., Chu, X., Zhou, X.-Z., & Yue, C. (2015). Substorm current wedge composition by wedgelets. *Geophysical Research Letters*, *42*, 1669–1676. https://doi.org/10.1002/2015GL063289

Newell, P. T., & Gjerloev, J. W. (2011a). Evaluation of SuperMAG auroral electrojet indices as indicators of substorms and auroral power. *Journal of Geophysical Research*, *116*, A12211. https://doi.org/10.1029/2011JA016779

Newell, P. T., & Gjerloev, J. W. (2011b). Substorm and magnetosphere characteristic scales inferred from the SuperMAG auroral electrojet indices. *Journal of Geophysical Research*, *116*, A12232. https://doi.org/10.1029/2011JA016936

Ngwira, C. M., Pulkkinen, A. A., Bernabeu, E., Eichner, J., Viljanen, A., & Crowley, G. (2015). Characteristics of extreme geoelectric fields and their possible causes: Localized peak enhancements. *Geophysical Research Letters*, *42*, 6916–6921. https://doi.org/10.1002/2015GL065061

Ngwira, C. M., Sibeck, D. G., Silveira, M. D. V., Georgiou, M., Weygand, J. M., Nishimura, Y., & Hampton, D. (2018). A study of intense local d*Bdt* variations during two geomagnetic storms. *Space Weather*, *16*, 676–693. https://doi.org/10.1029/2018SW001911

Nikitina, L., Trichtchenko, L., & Boteler, D. H. (2016). Assessment of extreme values in geomagnetic and geoelectric field variations for Canada. *Space Weather*, *14*, 481–494. https://doi.org/10.1002/2016SW001386

Oliveira, D. M., Arel, D., Raeder, J., Zesta, E., Ngwira, C. M., Carter, B. A., et al. (2018). Geomagnetically induced currents caused by interplanetary shocks with different impact angles and speeds. *Space Weather*, *16*, 636–647. https://doi.org/10.1029/2018SW001880

Palin, L., Jacquey, C., Opgenoorth, H., Connors, M., Sergeev, V., Sauvaud, J.-A., et al. (2015). Three-dimensional current systems and ionospheric effects associated with small dipolarization fronts. *Journal of Geophysical Research: Space Physics*, *120*, 3739–3757. https://doi.org/10.1002/2015JA021040

Runov, A., Angelopoulos, V., Sitnov, M. I., Sergeev, V. A., Bonnell, J., McFadden, J. P., et al. (2009). THEMIS observations of an earthward propagatingdipolarization front. *Geophysical Research Letters*, *36*, L14106. https://doi.org/10.1029/2009GL038980

Runov, A., Angelopoulos, V., Zhou, X.-Z., Zhang, X.-J., Li, S., Plaschke, F., & Bonnell, J. (2011). A THEMIS multicase study of dipolarization fronts in the magnetotail plasma sheet. *Journal of Geophysical Research*, *116*, A05216. https://doi.org/10.1029/2010JA016316

Singer, H. J., Matheson, L., Grubb, R., Newman, A., & Bouwer, S. D. (1996). Monitoring space weather with the GOES magnetometers. In E. R. Washwell (Ed.), SPIE Conference Proceedings (Vol. 2812, pp. 299–308). Bellingham, Wash: GOES-8 and Beyond, SPIE.

Syrjäsuo, M. T., & Donovan, E. F. (2004). Diurnal auroral occurrence statistics obtained via machine vision. *Annales Geophysicae*, *22*, 1103–1113. https://doi.org/10.5194/angeo-22-1103-2004

Viljanen, A. (1997). The relation between geomagnetic variations and their time derivatives and implications for estimation of induction risks. *Geophysical Research Letters*, *24*, 631–634. https://doi.org/10.1029/97GL00538

Viljanen, A., Nevanlinna, H., Pajunpää, K., & Pulkkinen, A. (2001). Time derivative of the horizontal geomagnetic field as an activity indicator. *Annales Geophysicae*, *19*(9), 1107–1118. https://doi.org/10.5194/angeo-19-1107-2001

Viljanen, A., & Tanskanen, E. (2011). Climatology of rapid geomagnetic variations at high latitudes over two solar cycles. *Annales Geophysicae*, *29*, 1783–1792. https://doi.org/10.5194/angeo-29-1783-2011

Viljanen, A., Tanskanen, E. I., & Pulkkinen, A. (2006). Relation between substorm characteristics and rapid temporal variations of the ground magnetic field. *Annales Geophysicae*, *24*, 725–733. https://doi.org/10.5194/angeo-24-725-2006

Vorobev, A., Pilipenko, V., Sakharov, Y., & Selivanov, V. (2019). Statistical relationships between variations of the geomagnetic field, auroral electrojet, and geomagnetically induced currents. *Solar-Terrestrial Physics*, *5*, 35–42. https://doi.org/10.12737/stp-51201905